Eocene-Oligocene tectonics and kinematics of the Rhine-Saone Continental Transform Zone (eastern France)

Olivier Lacombe, J. Angelier, D. Byrne, J. M. Dupin

TECTONICS, VOL. 12, NO. 4, PAGES 874-888, AUGUST 1993

EOCENE-OLIGOCENE TECTONICS AND KINEMATICS OF THE RHINE-SAONE CONTINENTAL TRANSFORM ZONE (EASTERN FRANCE)

O. Lacombe, J. Angelier, D. Byrne, and J. M. Dupin
Tectonique Quantitative, Université Pierre et Marie Curie, Paris, France

Abstract. A tectonic analysis of brittle deformation was performed in the Rhine-Saône transform in order to decipher and understand the deformation processes in a typical continental transfer zone. Cenozoic major and minor fault patterns are described, and brittle structures are interpreted in terms of paleostress orientations. The Eocene N-S compression related to Africa-Eurasia convergence is marked mainly by strike-slip faults. It was followed by a major phase of crustal extension, mainly Oligocene in age, related to the west European rifting. This extensional phase is expressed by normal faults, tension gashes, and extensional strike-slip faults which are especially abundant in the transform zone. These two events are found to be quite different in terms of distribution of horizontal stress trajectories. The trend of σ1 axes is very homogeneous for the N-S compression, whereas σ3 orientations associated with the major extension vary from E-W in most of the Rift system to NW-SE within the transform zone. Finally, the Mio-Pliocene tectonic emplacement of the Jura fold-and-thrust belt is marked in the field by strike-slip faults associated with a well-defined trend of σ1 oriented W-NW-E-SE to NW-SE. The preexisting basement fracture pattern between the grabens was also considered in order to estimate which faults were likely to have been reactivated during the Oligocene transform kinematics, and the theoretical shear motion on these inherited fault surfaces, when submitted to E-W extension, was calculated. Left-lateral/extensional reactivation of a preexisting 60°N trending fault system in the brittle upper crust is likely to have accommodated the shear strain arising between the rift segments in response to crustal stretching. Two independent numerical modelings, based on distinct element and finite element analyses, respectively, enabled us to verify and to refine the hypothesis of transform kinematics related to E-W extension and inducing regional perturbations of extensional stress trajectories. The overall mechanism and the transtensional kinematics of the Rhine-Saône transform zone are thus tightly constrained. The inherited crustal anisotropy, the large-scale perturbations of extensional stress trajectories, and the development of distributed brittle deformation within the sedimentary cover are found to play a major role in the tectonic evolution of continental rift-transform systems.

INTRODUCTION

The development of continental rifts illustrates the early stages of continental extension and breakup. From a mechanical point of view, rifting is usually associated with discrete transfer or transform zones which accommodate deformation and release the shear strain arising from the offset of the rift segments due to crustal stretching. Examples of such transform zones were identified and documented in previous works [e.g., Illies, 1972, 1974; Tapponnier and Varet, 1974; Freund, 1974; Bergerat, 1977; Kazmin, 1980; Garfunkel, 1981; Ron and Eyal, 1985; Ebinger, 1989; Chorowicz , 1989].

Tectonic and paleostress analyses on exposed fossil transform zones provide a good opportunity to reliably define and interpret the stress field around continental transform faults. Stress distribution may be further used to constrain numerical models of the mechanics of continental transform zones, as is pointed out in other papers [Dupin, 1990; Byrne et al., 1992]. In spite of some major differences between oceanic and continental transform faulting, such as different mechanical behavior of continental and oceanic lithospheres and greater importance of crustal anisotropy inherited from earlier orogenic history within continental basement, this approach also may be useful in understanding stress and deformation patterns at ridge-ridge transforms.

During Cenozoic times, the west European platform was cut by a system of approximately N-S trending grabens extending from the western Mediterranean to the North Sea. This system is called the west European Rift. It is divided into several segments linked by intracontinental transform zones [Laubscher, 1970; Illies, 1972, 1981; Rat, 1974, 1978; Bergerat, 1977; Bergerat and Chorowicz, 1981]. The "Burgundy gate" which connects the Saône and Rhine grabens is representative for such a rift-rift transform (Figure 1). Although the nature of transform in this area is beyond doubt, the actual kinematics of this continental transform zone and the associated paleostress pattern, as well as its relation to plate kinematics models proposed for the Africa-Eurasia convergence [Sengör, 1976; Tapponnier, 1977; Le Pichon et al., 1988], are still subject to contrasting interpretations [Bergerat, 1977; Lacombe et al., 1990a; Lacombe and Dupin, 1991].

In the Rhinegraben, tilted block geometry, subsidence data as well as numerical modelings [Villemin et al., 1986] suggest that the amount of extension did not exceed 5 ± 2 km; in the Bresse graben, seismic reflection data collected along the Jura-Bresse ECORS traverse lead to a first estimate of 2 km of crustal extension [Bergerat et al., 1990]. This means that compared with 50-70 km wide zones of extension as seen on the seafloor and from which the term "transform" was derived, the Rhine and Saône rift-transform system only appears as a 2 to 5-km-wide zone of extension without significant crustal creation. As a consequence, the terms "transfer zone" or "accommodation zone" may be therefore more appropriate than "transform zone". We decided, however, to keep the name "Rhine-Saône transform zone" which has been already proposed and widely used by previous authors [e.g., Illies, 1972; Contini and Théobald, 1974; Bergerat, 1977].

The aim of this paper is to present new structural data combined with a reanalysis of previous results, in order to provide new constraints on the Eocene-Oligocene kinematics of the continental Rhine-Saône transform zone. We also incorporate numerical modeling in an attempt to check our earlier hypotheses regarding regional-scale paleostress perturbations related to transform kinematics [Lacombe et al., 1990a]. First, we present tectonic data related to the Cenozoic

Paper number 93TC00233.
0278-7407/93/93TC-00233$10.00

geologic evolution of the transform zone. These data are quantitatively interpreted in terms of paleostress orientations (Figures 2, 3, and 4). Second, on the basis of the regional paleostress field and regional structures we constrain the Eocene-Oligocene tectonics and kinematics of the Rhine-Saône transform zone. A dynamic and kinematic model is proposed for this time interval and compared with numerical and experimental models. It is important to note that as a consequence of the scope of the paper, tectonic features related to post-Oligocene events (especially the Mio-Pliocene Alpine compression associated with building of the Jura Mountains: Figure 4) will be briefly described but will not be discussed in detail further because transform kinematics presumably had ceased by then.

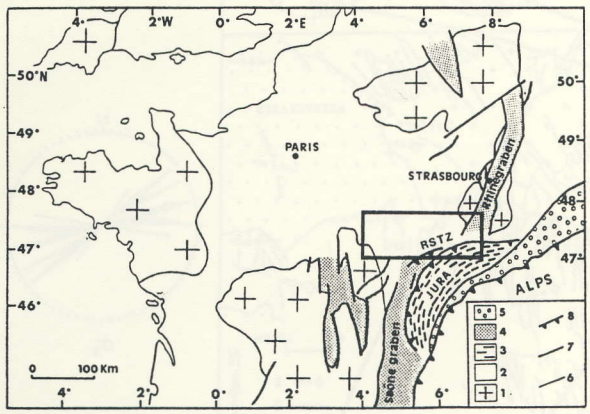

Fig. 1. Schematic map of the western European platform showing the location of the area investigated (frame). Key: 1, Hercynian basement; 2, Sedimentary formations; 3, "Fold-and-thrust" system of Jura Mountains (fold axes as dashed lines); 4, Cenozoic rifts; 5, Alpine foreland basin; 6, Stratigraphic contacts; 7, Main faults and 8, Thrusts (barbs on upthrust side). RSTZ: Rhine-Saône Transform Zone.

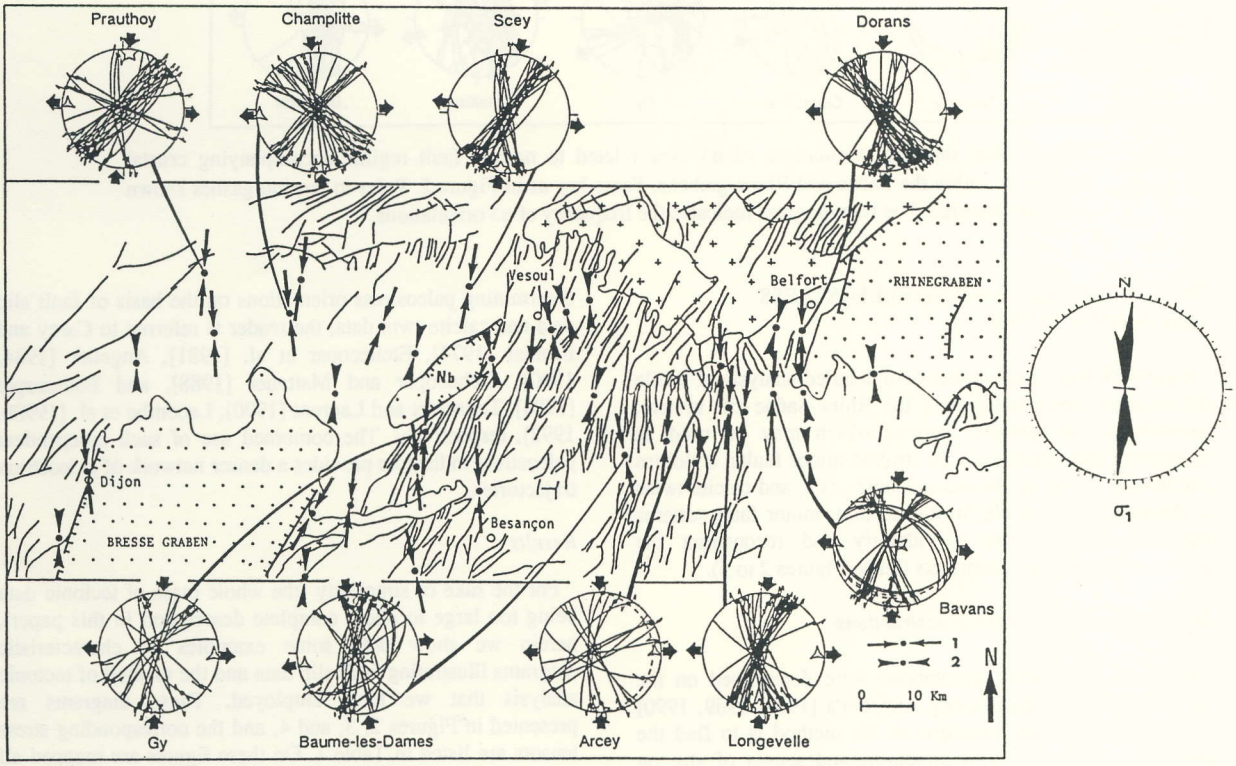

Fig. 2. Map showing orientations of σ1 axes related to the strike-slip fault regime marking the Eocene Pyrenean-Alpine compression. Unpatterned areas: Mesozoic sedimentary formations; Dotted pattern: Cenozoic rifts. Crossed pattern: Paleozoic-Triassic formations. Nb: Noidans basin. Key : 1, Paleostress orientations determined in this study and 2, Paleostress orientations compiled from literature [Bergerat, 1987; Villemin and Bergerat, 1987; Larroque and Laurent, 1988]. Fault slip data: diagrams (lower hemisphere, equal area projection) with faults as thin curves and slickenside lineations as dots with double arrows (left- or right lateral) or simple ones (centrifugal-normal; centripetal-reverse). Paleostress directions as empty stars with five points (maximal compressive stress σ1), four points (middle stress σ2), or three points (minimal stress σ3); Direction of extension or compression as large black arrows. For characteristics of stress tensors, refer to Table 1. The rose diagram indicates the frequency of σ1 orientations.

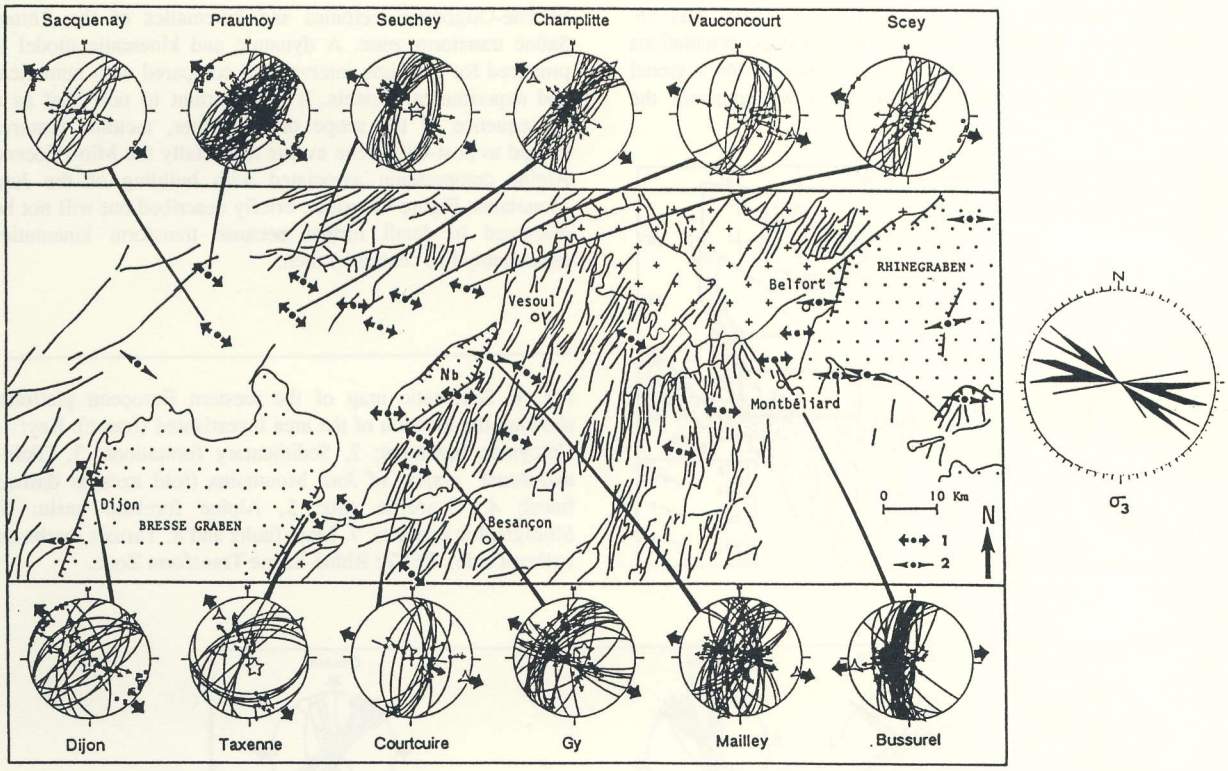

Fig. 3. Map showing orientations of σ3 axes related to normal fault regime accompanying crustal extension within the Saône and Rhine grabens. Same key as in Figure 2. Poles to tension gashes shown as empty squares. The rose diagram indicates the frequency of σ3 orientations.

TECTONIC ANALYSES AND PALEOSTRESS RECONSTRUCTIONS

Fieldwork was concentrated on a detailed analysis of brittle deformation structures around the Rhine-Saône rift system, particularly, on tectonic features which may be used as paleostress indicators, such as striated minor faults, stylolites and tension gashes at the macroscopic scale, and calcite twins at the microscopic scale. In this section, minor fault patterns are analyzed in order to identify and reconstruct the successive Cenozoic paleostress fields (Figures 2 to 5).

Methods for Paleostress Reconstructions

Regional paleostress orientations were determined on the basis of fault slip data using Angelier's [1984, 1989, 1990] inverse methods. The principle of the method is to find the best fit between observed directions and senses of slip on faults and theoretical shear stress induced on these planes by a common stress tensor (the solution of the inverse problem). For calcite twins, the inversion of crystallographic data in order to obtain the regional stress was carried out from oriented samples collected in Mesozoic and Oligocene limestones by using the computer-based method developed by Etchecopar [1984]. Both analyses yield the orientations of the three principal stresses σ1, σ2, and σ3, with $\sigma1 \geq \sigma2 \geq \sigma3$ (compressional stress considered as positive) and the Φ ratio between differential stress magnitudes [$\Phi = (\sigma2-\sigma3)/(\sigma1-\sigma3)$, with $0 \leq \Phi \leq 1$]. For a further discussion on the methods of determining paleostress orientations on the basis of fault slip data and calcite twin data, the reader is referred to Carey and Brunier [1974], Etchecopar et al. [1981], Angelier [1984, 1990], Etchecopar and Mattauer [1988], and Etchecopar [1984], Tourneret and Laurent [1990], Lacombe et al. [1990b, 1992], respectively. The combined use of such independent paleostress indicators provides a denser network of paleostress trajectories.

Results

For the sake of simplicity (the whole mass of tectonic data being too large to allow complete description in this paper), herein we show only some examples of characteristic diagrams illustrating fault slip data and the method of tectonic analysis that we have employed. These diagrams are presented in Figures 2, 3, and 4, and the corresponding stress tensors are listed in Table 1. On these figures are mapped all the paleostress orientations determined at each site from striated faults, tension gashes and calcite twins, or compiled from the literature for deformation in Cenozoic times [Villemin, 1986; Bergerat, 1987; Villemin and Bergerat, 1987; Larroque and Laurent, 1988]. The paleostress fields that we reconstructed from Cenozoic fault patterns are described below.

Cenozoic Paleostress Fields in the Rhine-Saône Transform

N-S "Eocene" compression. A regional paleostress system characterized by N-S horizontal compression associated with

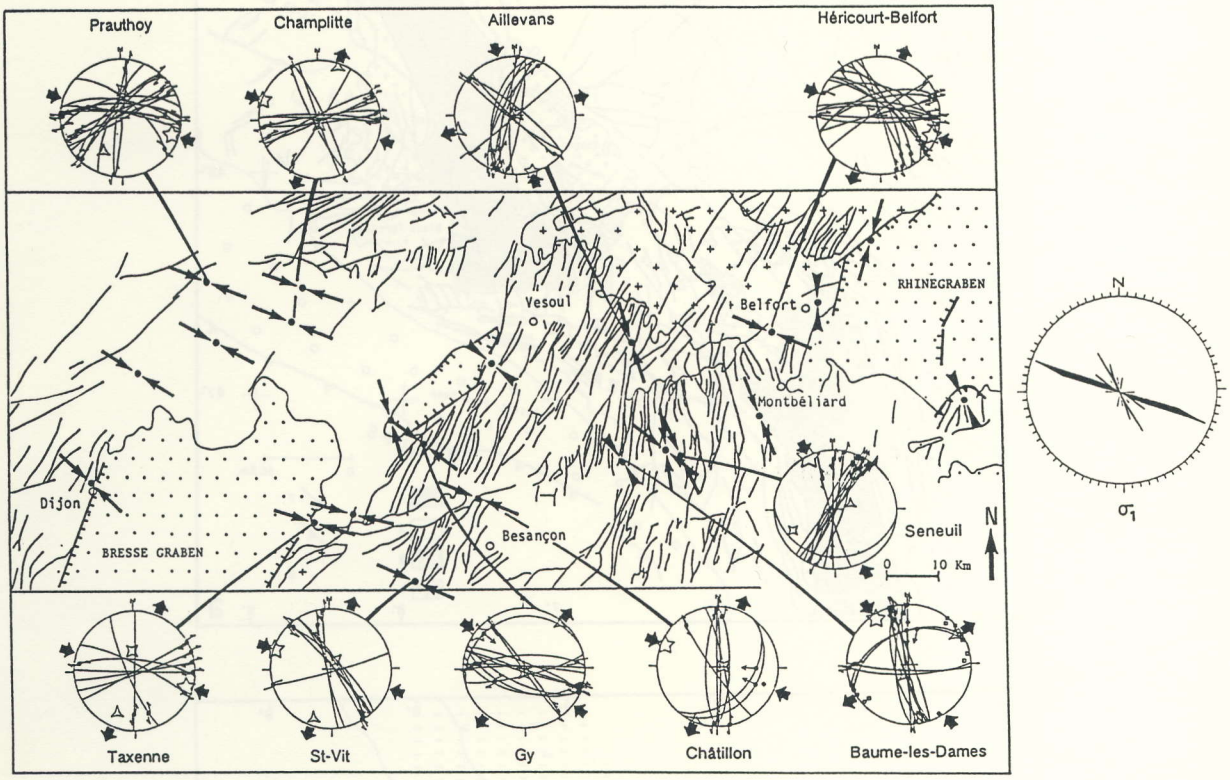

Fig. 4. Map showing orientations of σ1 axes related to the strike-slip fault regime marking the Mio-Pliocene Alpine compression. Same key as in Figure 2. Poles to tension gashes shown as empty squares. The rose diagram indicates the frequency of σ1 orientations.

E-W extension was determined in about 40 sites. As shown in Figure 2, related structures mainly consist of left-lateral strike-slip faults whose trends range from 10°N to 60°N and right-lateral strike-slip faults whose trends range from 110°N to 160°N. The shear motion on these faults is purely strike-slip or displays a reverse component. The trends of the computed σ1 axes are tightly clustered around N-S direction (Figure 2). This well-defined trend is consistent with σ1 orientations derived from stylolitic peaks. The age of this event is difficult to establish in the absence of convenient Cenozoic outcrops. It could correspond either to the early Paleocene compressional phase which gave rise to basin inversion in NW Europe, as well as to break in sedimentation and erosional hiatus at the boundary between Mesozoic and Cenozoic sediments in the area under investigation [Ziegler, 1988, 1990], or to the late Eocene paroxysm of the Pyrenean compression which prevailed since the late Cretaceous until the late Eocene in the Pyrenees-Provence foreland [Mattauer and Mercier, 1980; Letouzey and Tremolieres, 1980; De Charpal et al., 1981; Arthaud and Seguret, 1981; Letouzey, 1986; Bergerat, 1987; Lacombe et al., 1992]. In the absence of more precise stratigraphic dating, we propose that the observed compressional features associated with submeridian σ1 orientations and which clearly predated development of the Saône and Rhine grabens are related to the stresses exerted by the Pyrenean and Alpine orogens on their foreland since the late Cretaceous and mainly during the Eocene, in response to nearly N-S Africa-Eurasia convergence.

E-W to NW-SE "Oligocene" extension. A widespread extensional stress regime, with maximum principal stress σ1 vertical, was also reconstructed from many normal faults and calcite-filled tension gashes (Figure 3). Superposition criteria (successive slickenside lineations on fault planes) or cross-cutting relationships between faults or tension gashes suggest that this extensional event regionally postdates the episode of N-S compression previously related to Eocene. Moreover, this extension is prevalent close to the Saône and Rhine grabens, and, where outcrop conditions permit, consistent normal faulting is also observed within the Oligocene fill of the grabens (Figures 3 and 5a). As a consequence, it is likely that this extensional tectonics is related to the west European rifting event [Rat, 1976; Bergerat, 1987; Larroque and Laurent, 1988], that started in the late Eocene within the southern Rhinegraben [Villemin et al., 1986; Dewey and Windley, 1988; Ziegler, 1992], and was responsible for major tectonism and crustal stretching within the Saône and Rhine grabens during the Oligocene. The computed σ3 directions, presented in Figures 3 and 5b, are not homogeneous in trend across the area. In contrast to the overall E-W direction of extension in the rift system (as indicated by the systematic analysis of the growth of gypsum fibers in the Mulhouse Oligocene basin by Larroque and Ansart [1985]), paleostress

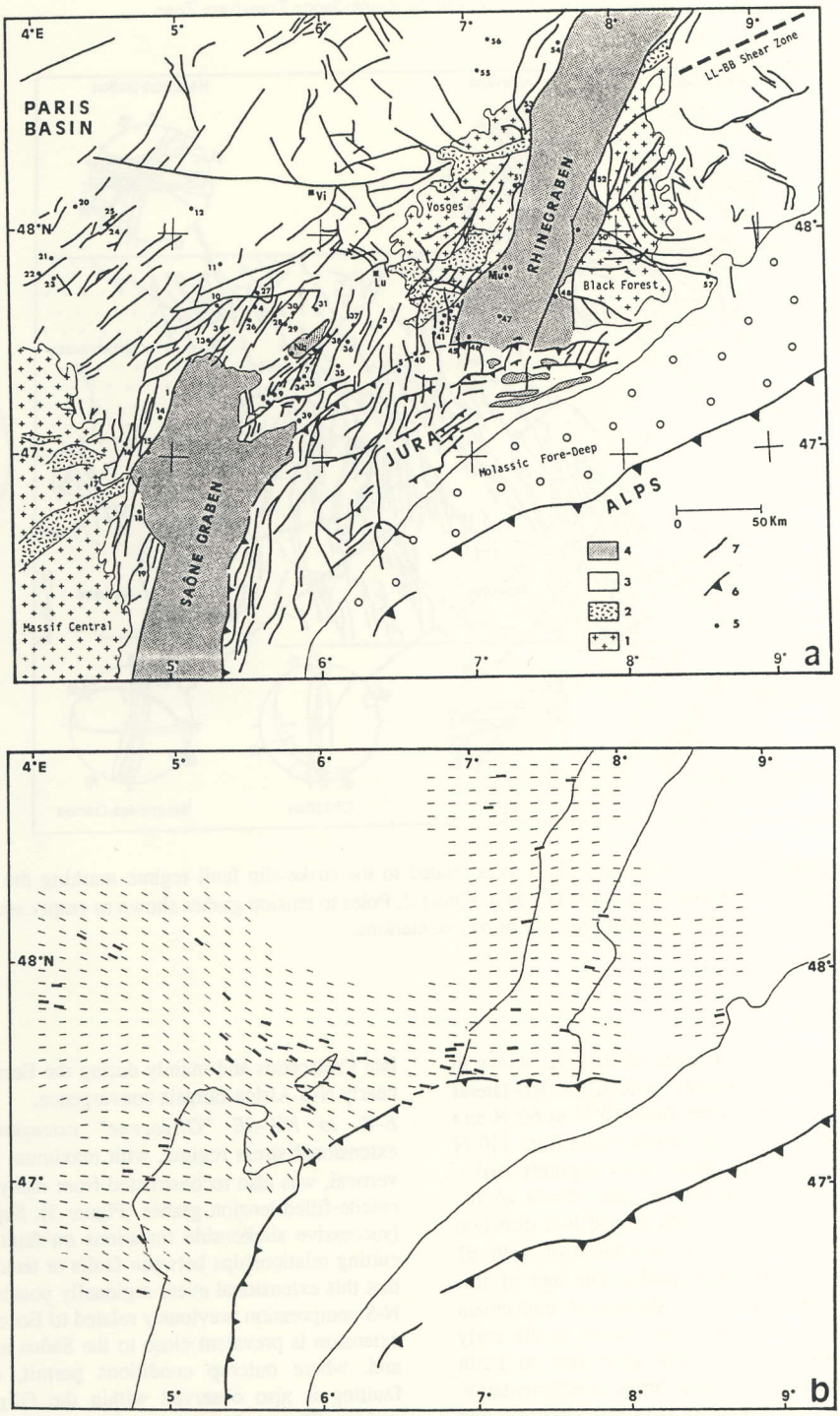

Fig. 5. (a) Structural map of the Rhine-Saône rift system, with location of sites of data collection. Key : 1, Hercynian basement; 2, Permo-Carboniferous basins and synclines (note the predominant 60°N-70°N trend); 3, Mesozoic sedimentary formations; 4, Main Cenozoic grabens; 5, Sites of data collection; 6, Main faults; 7, Thrusts (barbs on upthrust side); Lu, Luxeuil; Vi, Vittel; Mu, Mulhouse; LL-BB, Lalaye-Lubine-Baden Baden shear zone; and Nb, Noidans basin. (b) The $\sigma 3$ trajectories related to the extensional stress regime responsible for the development of the Saône and Rhine grabens (coordinates of sites and trends and plunges of $\sigma 3$ are listed in Table 2). The heavy dashes represent local $\sigma 3$ orientations determined from geologic stress indicators, the slight ones the averaged trajectories (computer-based smoothing method by J.C. Lee and J. Angelier, Interpolation and Smoothing methods for regional distribution of directional data : paleostress trajectories as an example, submitted to *Mathematical Geology*, 1993). Note the heterogeneous distribution of stress in the vicinity of the presumed transform zone contrasting with the homogeneous stress regime of the grabens.

TABLE 1. Main Characteristics of Paleostress Tensors Computed Using Fault Slip Data (Diagrams Shown in Figures 2 to 4)

Site	σ1 Trend-Plunge	σ2 Trend-Plunge	σ3 Trend-Plunge	Φ	N	ANG (°)
N-S Compression (Figure 2)						
Prauthoy	006-03	127-85	276-05	0.4	30	10
Champlitte	174-00	032-80	265-06	0.5	26	11
Scey	189-05	033-84	279-02	0.48	28	12
Dorans	182-04	354-86	092-01	0.27	33	10
Gy	185-09	321-78	093-08	0.59	17	17
Baume	350-07	110-76	259-12	0.35	24	18
Arcey	181-02	282-78	090-12	0.40	14	12
Longevelle	185-11	314-73	093-13	0.48	27	12
Bavans	184-03	072-83	275-07	0.26	24	7
E-W to NW-SE Extension (Figure 3)						
Sacquenay	210-66	039-23	307-03	0.38	8	15
Prauthoy	035-85	221-06	131-01	0.3	74	15
Seuchey	076-83	210-05	301-05	0.45	31	7
Champlitte	136-76	040-01	310-13	0.3	39	22
Vauconcourt	310-82	202-03	111-08	0.47	13	9
Scey	344-85	197-04	107-03	0.22	20	20
Dijon	181-83	046-05	316-05	0.31	18	11
Taxenne	149-75	056-01	326-15	0.3	16	6
Courtcuire	328-83	200-05	109-06	0.4	13	7
Gy	059-74	209-14	301-08	0.27	29	15
Mailley	309-85	196-02	106-05	0.21	39	11
Bussurel	043-77	170-08	262-10	0.37	38	21
E-W to NW-SE Compression (Figure 4)						
Prauthoy	113-07	005-69	206-20	0.5	17	14
Champlitte	290-02	182-83	020-07	0.4	10	9
Aillevans	165-01	054-87	255-03	0.55	12	9
Héricourt	113-09	294-81	203-00	0.29	18	13
Taxenne	108-12	355-62	204-25	0.3	8	12
Saint-Vit	290-03	031-76	199-13	0.29	9	8
Gy	309-04	181-83	039-05	0.29	11	17
Châtillon	292-07	084-82	202-04	0.32	8	14
Baume	326-08	202-76	058-12	0.34	12	13
Seneuil	335-03	244-23	072-67	0.00	14	12

Stress axes: trend and plunge, in degrees. Φ ratio, defined in text; N, number of fault slip data; ANG, average angle between computed shear stress and observed slickenside lineation, in degrees.

indicators yield directions of extension ranging from E-W to NW-SE within the transform zone (Figures 3 and 5b). The regional significance of these deviations of stress orientations and their relation to Rhine-Saône transform kinematics will be discussed below.

Mio-Pliocene W-NW-E-SE compression. According to relative chronology data, a W-NW-E-SE compression characterizes the last tectonic event that we could recognize in the field. The trend of the σ1 axes computed from fault slip and calcite twin data is nearly constant, W-NW-E-SE to NW-SE. This compression is characterized by left-lateral strike-slip faults whose trends range from 120°N to 160°N, and right-lateral strike-slip faults with trends from 20°N to 90°N (Figure 4). Some of these faults correspond to reactivated fault planes inherited from the previous N-S compression and/or the E-W to NW-SE extension, thus providing evidence that this event postdated the main extensional phase. Although the exact age of this event cannot be established with certainty, the relative chronology criteria as well as the orientation of the main direction of σ1 suggest that it was very probably contemporaneous with the westward thrusting of Jura [Caire, 1974; Bergerat, 1987], whose frontal thrust elements overrode the eastern margin of the Bresse graben during Mio-Pliocene and were sealed by Pliocene sediments [Chauve et al., 1988; Guellec et al., 1990].

Geometry and Tectonic Significance of Eocene-Oligocene Minor and Major Fault Patterns Within the Rhine-Saône Transform Zone

The determination of the successive regional paleostresses based on fault slip data sets thus enabled us to decipher the complex minor fault systems within the transform zone. More particularly, it allowed us to identify and then separate Eocene-Oligocene fault patterns from the Mio-Pliocene fault patterns that developed after the transform motion had ceased. In this section, we thus only focus on Eocene-Oligocene faulting, without considering Mio-Pliocene fault systems.

At a regional scale (Figure 5a), the sedimentary cover between the Saône and the Rhine grabens displays a dense, complex pattern of major en échelon 35°N trending fractures or shear zones with a predominant sinistral sense of displacement (Figures 2, 3, 4, and 5a). Some of these regional-scale faults display a pure strike-slip sinistral motion, whereas others additionally display a significant normal motion (both left-lateral and normal), as shown by the contrast of outcropping formations on opposite sides of the faults, thus cutting the Jurassic formations into small, narrow NE-SW grabens like the shallow, Noidans Oligocene basin. Stress-strain partitioning thus arose and resulted in mixed families of oblique-slip faults and pure strike-slip faults. This fault pattern differs from tectonic features of the rift system itself where large-scale normal dip-slip faults clearly mark the faulted borders of the Saône and Rhine grabens (Figures 1 and 5a).

In order to allow an efficient comparison between these major fault patterns and the minor faults that we found to be related to the Eocene-Oligocene tectonisms, we correlated the geometries of the measured individual fault planes, slickenside lineations and senses of motion by plotting the dip of each fault plane measured in the field versus the pitch of the striae observed on it (Figure 6). The senses of relative motion on a fault plane are thus easily identified as normal-dextral, normal-sinistral, reverse-dextral and reverse-sinistral. Three main pools of fault poles emerge from this diagram. The first one at the center of the diagram corresponds to normal dip-slip faults that are observed at various scales in the area of interest; they are similar to the major faults bordering the Saône and Rhine grabens and are related to the main extensional phase. The two other pools correspond to left- and right-lateral strike-slip faults. Motion on many of these faults, however, is not purely normal/dip-slip or purely strike-slip. Rather, some strike-slip faults experience oblique-slip, which makes them "extensional strike-slip faults" as shown by their normal component of shear (Figure 6) which is consistent with E-W extension. These extensional strike-slip faults differ from the pure or compressional strike-slip faults that clearly mark the pre-extensional Eocene N-S compression; their geometry resembles that of the 35°N major faults that crosscut the Jurassic plateaus of the transform zone. The minor and major 35°N trending extensional strike-slip faults are thus very probably related to the Oligocene evolution of the area (Figure 7).

In summary, paleostress reconstructions and analyses of the geometry of minor and major fault patterns unambiguously

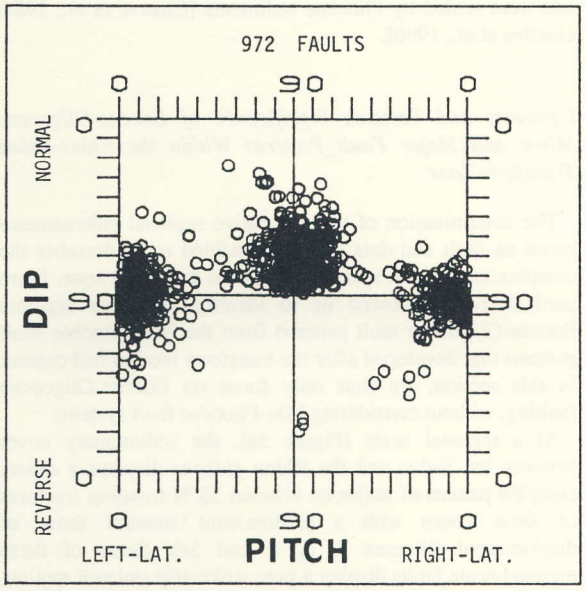

Fig. 6. Dip versus pitch diagrammatic representation of Eo-Oligocene fault slip data sets. The quadrants refer to normal-dextral, normal-sinistral, reverse-dextral, and reverse-sinistral sense of relative motion. The maximum at the center of the diagram corresponds to pure (dip-slip) normal faults. The two other maxima correspond to sinistral and dextral strike-slip faults. Note that extensional strike-slip faults can be detected according to their normal component of shear (see also Figure 7).

indicate polyphase tectonics for Eo-Oligocene times, as noted previously by Gelard [1979] and Bergerat [1987]. An early phase of deformation possibly related to the Eocene Pyrenean/Alpine compression gave rise to pure and reverse strike-slip faulting within the Rhine-Saône transform zone. This compressional phase was followed by a major phase of crustal extension that started during the late Eocene within the Rhinegraben but occurred mainly during the Oligocene in the whole of the west European Rift and presumably controlled the opening of the Rhine/Saône rift system. This E-W to NW-SE extension expressed in the field by tension gashes and normal dip-slip faults, but also by minor and major extensional strike-slip faults that developed widespread within the transform zone. Transform kinematics and coeval major crustal extension ceased by the late Oligocene-early Miocene, so that most of the younger (Miocene) subsidence within the Saône graben and the southern Rhinegraben should be interpreted in terms of thermal subsidence rather than in terms of the persistence of crustal extension.

KINEMATIC CONSTRAINTS DERIVED FROM OBLIQUE REACTIVATION OF BASEMENT DISCONTINUITIES

Because of its complex orogenic history, continental lithosphere generally exhibits pervasive strength anisotropies caused by preexisting fractures or zones of weakness. During rifting of the continental crust, tensional forces will reactivate some of these preexisting zones of weakness depending on their orientations relative to the newly imposed stress field. We examined the preexisting fracture pattern in the basement between the Saône and Rhine grabens in order to evaluate which faults were likely to have been reactivated during Oligocene E-W extension.

Variscan and Late Variscan Fault Pattern

The pre-Mesozoic fault pattern in the crust of NE France has been documented from geologic data [Arthaud and Matte, 1975, 1977; Müller et al., 1984; Ziegler, 1986; Wickert and Eisbacher, 1988; Eisbacher et al., 1989], geophysical investigations [Edel et al., 1975; Edel and Fluck, 1989] and satellite imagery [Bergerat and Chorowicz, 1981]. The main characteristics of the crust in this area result from the Variscan collisional orogeny (400 to 320 Ma) [Ziegler, 1986]. The tectonic features related to this orogeny are crustal-scale 35°N and 60°N trending strike-slip faults that developed during the late Visean and Namurian (350-325 Ma), and 60°N to E-W striking south or north verging major thrusts [Matte, 1986a,b; Wickert and Eisbacher, 1988; Edel and Fluck, 1989]. For example, the Lalaye-Lubine-Baden Baden shear zone (Figure 5a) is a major fault system that crops out as a steep, southward-dipping shear zone and shows evidence of a multiphase movement history [Wickert and Eisbacher, 1988].

The Variscan orogeny was followed by postorogenic extension in late Carboniferous times (320 to 290 Ma) [Eisbacher et al., 1989] and Permian times (290 to 250 Ma), which induced development of E-NE-W-SW to E-W trending collapse basins [Ziegler, 1980, 1990]. These basins principally formed along major Carboniferous fault zones trending 60°N, in the French Massif Central [Bles et al., 1989], the Vosges, and in the southern Black Forest [Müller et al., 1984]. For example, in the southern Vosges, the 60°N trending Luxeuil fault system (see location on Figure 5a) was reactivated in Permian times and controlled deposition of thick Permian sandstones and felsic volcanics [Edel and Fluck, 1989].

Thus, a complex fault system involving linked faults with various dips (thrust sutures, wrench and normal fault zones trending approximately 60°N) occurs in the basement beneath the Rhine-Saône transform zone. Such 60°N-oriented discontinuities constituted crustal weaknesses capable of being reactivated preferentially during subsequent tectonic events. For the sake of simplicity, this basement fault system will be referred to as a single 60°N trending fault zone in the following sections of this paper.

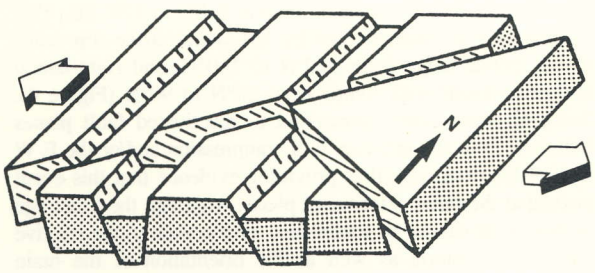

Fig. 7. Theoretical sketch of geometrical relationships and mechanical compatibility between extensional strike-slip faulting and pure normal faulting under stress boundary conditions of E-W extension.

Oblique Reactivation of Basement Fractures Under E-W Extension

Clay and sand laboratory experiments on continental rift/transform systems [e.g., Elmohandes, 1981] provide some basis to interpret the regional structural setting of the Rhine-Saône transform zone. With a main E-W extension during the Oligocene (Figures 3 and 5b), a major inherited basement fault system that trends 60°N-70°N beneath the transform zone, and mixed sets of 35°N trending, en échelon, oblique-slip and pure strike-slip faults in the cover, the structural pattern resembles the sand-box experiments on oblique extension by Tron and Brun [1991]. In these experiments, uniaxial stretching was applied oblique to the external boundaries of a brittle-ductile model (two-layer slabs of sand and silicone above two diverging basal sheets separated by a discontinuity). For boundary conditions involving a low angle (about 15-25°) between the basement discontinuity (the 60°N-70°N basement fault) and the applied stretching vector (E-W) (Figure 8), their modeling predicts formation of steeply-dipping, en échelon faults in the sedimentary cover, in response to transtensional reactivation of the discontinuity at the bottom of the model (Figure 8). These en échelon faults develop at 45°-60° from the stretching direction (i.e., not perpendicular to it) and display normal/strike-slip or pure strike-slip motions. The experimental models thus exhibit a structural fracture pattern very similar to that observed within the Rhine-Saône transform zone (Figures 5a and 8). Consequently, we suggest that the fault pattern within the Rhine-Saône transform system conforms to regional-scale transtensional deformation, caused by the extensional reactivation of a basement fault trending oblique to the direction of extension.

The expected oblique reactivation of a basement weakness zone and the related development of extensional strike-slip faults in the overlying cover between the Saône and Rhine graben may be checked by the calculation of the theoretical shear stress along available preexisting 35°N and 60°N trending planes with various dips, submitted to E-W extension. Although frictional sliding controls the effective reactivation of inherited faults [e.g., Celerier, 1988], friction was neglected in a first approximation, because it does not influence the orientation of the striae on the reactivated fault surfaces. This calculation, based on Wallace-Bott's principle according to which slip on a fault surface occurs parallel to the maximum shear stress, is developed in the appendix. As one may expect, such a calculation predicts in most cases a left-lateral/normal motion along 35°N as well as 60°N planes. From the theoretical point of view, the dip of the 60°N basement discontinuity is found to slightly influence the orientation of the theoretical striae (appendix), and also the possibility of the fault plane to be reactivated (frictional sliding), but does not modify the general conclusion : whatever its actual dip, the 60°N trending fault system is reactivated as a left-lateral/normal fault zone during the E-W extension, and the predicted orientations of oblique slip (appendix) are compatible with the results of statistical analysis of actual fault slip geometry (Figure 6).

Following Bergerat [1977], we propose that the development of the Saône and Rhine grabens was associated with a regional wrench movement at depth along a preexisting 060° basement fault system. This fault system acted as a transform zone during Oligocene rifting and accommodated the resulting shear strain between the grabens. However, we have found no evidence of dominant N-S compression within the transform zone contemporaneous with E-W extension within the grabens [Contini and Theobald, 1974; Bergerat, 1977]. Geometrical and mechanical considerations based on fault patterns in the cover and in the basement, and reconstructions of paleostress orientations, rather suggest that the overall E-W extension produced along the 60°N basement fault system a component of transverse (oriented NW-SE) extension, making the resulting transform motion extensional strike-slip in the cover (Figure 9). The transform motion would have been purely strike-slip if extension had trended 060° (or if the basement fault zone had trended 90°N). This oblique extension is corroborated in the field by the development within the transform zone of small, NE-SW trending grabens such as the Noidans Oligocene basin (Figures 2, 3, 4, and 5a) which are clearly associated with local NW-SE directed extension. A model of pure strike-slip motion under a regional stress field dominated by N-S compression [Bergerat, 1977] (Figure 10a) fails to explain development of such a basin.

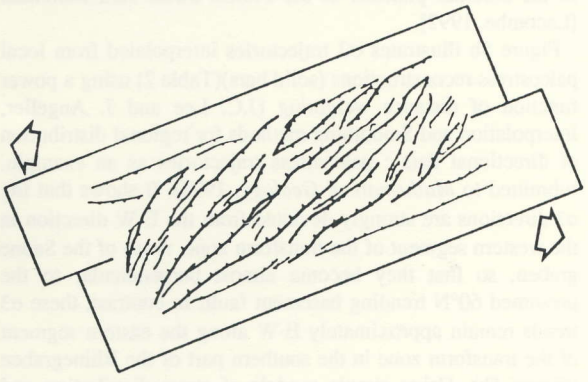

Fig. 8. Top view of a laboratory sand-box model on oblique reactivation of a preexisting basement discontinuity showing development of en échelon faults in the overlying cover. The angle between the stretching vector (large unshaded arrows) and the basement discontinuity is about 30° [after Tron and Brun, 1991]. This model exhibits a left-lateral extensional fault pattern very similar to that observed in the field (compare with Figure 5a).

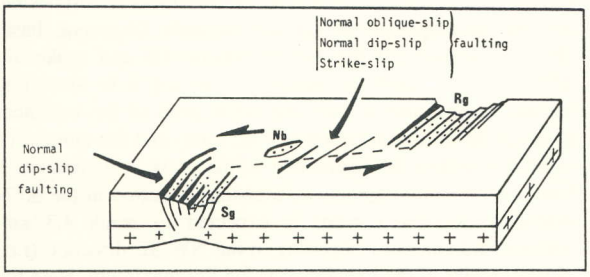

Fig. 9. Schematic block diagram illustrating the interpretative kinematic evolution of the transform zone, especially the resulting transtensional deformation in the sedimentary cover. Key : Rg, Rhinegraben; Sg, Saône graben and Nb, Noidans basin.

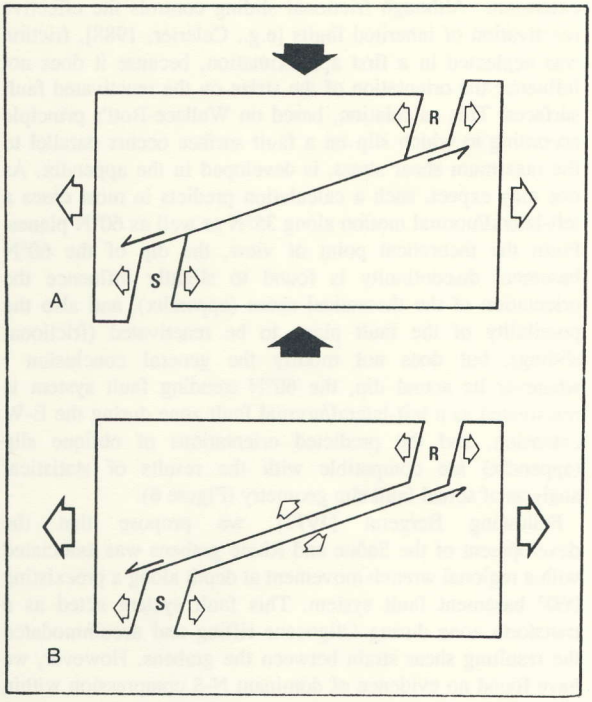

Fig. 10. Comparison of the previous basement model of Bergerat [1977] and the model proposed in this paper for the Rhine-Saône transform zone. (a) Graben formation associated with pure strike-slip motion along a 60°N trending basement fault, under regional N-S to 20°N compression. (b) Graben formation associated with wrench /extensional motion along a 60°N trending basement fault as a consequence of its oblique reactivation under actual E-W extension. The N-S part of the model is fixed (confining pressure) but not dominated by N-S compression as in (a).

In terms of rigid block kinematics, the model that best fits the structural data thus involves oblique left-lateral reactivation of a 60°N trending basement fault under E-W extension (Figure 10b), resulting in extensional sinistral strike-slip faulting in the cover (Figure 9). The model suggests that in addition to the predominant sinistral wrench movement that accommodates crustal extension within the Saône and Rhine grabens, a transverse (NW-SE) extensional component of motion is likely to have occurred (Figure 10b). This oblique component of motion in the basement is responsible for the development of (1) the Noidans Oligocene basin (Figure 5a) and (2) the mixed oblique-slip and strike-slip 35°N "Riedel" faults at nearly 55° to the E-W stretching vector. Taking into account the 60°N trend of the basement fault (at 30° to the direction of extension) and the amount of extension within the Saône and Rhine grabens (maximum 5 km), the maximum amount of transferred motion in the 60°N direction (left-lateral slip) is expected to reach 4.3 km, whereas the amount of opening in the NW-SE direction (i.e., perpendicular to the transform) is 2.5 km maximum. Here the dip of the reactivated basement fault system plays a major role, because it controls the way these 2.5 km of oblique extension are accommodated within the cover, even though the transform motion is in all cases extensional left-lateral (see appendix). More particularly, the vertical versus horizontal displacements within the cover above the basement fault are highly dependent on the dip of this basement fault. The absence of large vertical displacements within the transform zone suggests that the reactivated inherited fault system should rather correspond to a low-dipping fault zone (with a presumed SE dip like most of the crustal structures inherited from the Variscan orogeny in this area) [Matte, 1986a], but the subsurface data are unfortunately too scarce to allow to constrain this dip precisely.

In conclusion, this study emphasizes that regional deformation mode and fracture directions were not only controlled by stress orientations at the boundaries of the system (i.e., N-S confining pressure and E-W extension) but also by the heterogeneity and the anisotropy of the brittle crust.

KINEMATIC CONSTRAINTS DERIVED FROM PERTURBATIONS OF EXTENSIONAL STRESS TRAJECTORIES

Kinematic constraints also arise from the existence of stress deviations related to the main extensional phase. The trends of $\sigma 1$ axes related to the Eocene compressional deformation are very homogeneous (Figure 2). In contrast, the trend distribution of the $\sigma 3$ axes related to the extensional phase is more complex (Figures 3 and 5b). Angular deviations from the E-W direction, ranging from 0° (E-W) to 45° clockwise (NW-SE), have been detected as indicated by the analysis of minor normal faulting and other paleostress indicators (see rose diagram, Figure 3). As most of the small-scale normal faults, which developed during this extension, are newlyformed (Figure 3), they should correspond to the local preferred direction of fracture within the sedimentary cover in response to local stress fields. The distribution of these deviations relative to the overall regional E-W trend of $\sigma 3$ consists of a progressive clockwise change from 90°N to 135°N north of the Saône graben. Although this distribution of paleostress trajectories is reported herein only for the northern side of the transform zone (Figure 5b), a consistent extensional paleostress field has been identified to the South in the external plateaus of the French-Swiss Jura Mountain [Lacombe, 1992].

Figure 5b illustrates $\sigma 3$ trajectories interpolated from local paleostress reconstructions (solid bars)(Table 2) using a power function of distance weighting (J.C. Lee and J. Angelier, Interpolation and Smoothing methods for regional distribution of directional data : paleostress trajectories as an example, submitted to *Mathematical Geology*, 1993). It shows that the $\sigma 3$ directions are strongly deviated from the E-W direction in the western segment of the transform zone north of the Saône graben, so that they become almost perpendicular to the presumed 60°N trending basement fault. In contrast, these $\sigma 3$ trends remain approximately E-W along the eastern segment of the transform zone in the southern part of the Rhinegraben (Figure 5b). Using simple models of stress distribution and perturbation along shear fractures [Ricou, 1978; Segall and Pollard, 1980; Rispoli, 1981; Xiaohan, 1983], we interpret these deviations of extensional stress as perturbations of the overall E-W extension due to regional-scale transform motion [Lacombe et al., 1990a].

Two independent numerical modelings of stress trajectories within the Rhine-Saône rift system were carried out in order to check and refine our interpretation of stress deviations

related to transform kinematics, in a general stress field dominated by E-W extension. These models, discussed in more detail in other papers [Dupin, 1990; Byrne et al., 1992], involve two different and complementary approaches : a distinct element analysis, which is appropriate for modelling discontinuous deformation in the basement (i.e., stress patterns and deformations associated with slip on a discrete basement fault) [Dupin, 1990], and a finite element analysis, suitable for modeling stresses and distributed displacements within the overlying, approximately continuous, sedimentary cover [Byrne et al., 1992]. The two-dimensional horizontal elastic models we used are physically simplified compared with the actual rheology distribution; also, they do not take into account coupling at depth between plate kinematics and thermomechanical deformations within the lithosphere during rifting [Fleitout and Froidevaux, 1982, 1983]. Despite these simplifications, however, our models are valid in terms of distribution and orientation of the stress field within the upper crust, because we consider only horizontal tectonic stresses resulting from plate divergence without implying anything about the mechanism (the driving forces) for lithospheric extension and rifting (i.e., passive or active rifting).

TABLE 2. Location of Sites Shown in Figure 5a and Trends and Plunges of the Minimum Horizontal Stress σ3 Related to Oligocene Extension

Site	Site Name	Latitude Nord	Longitude Est	σ3 Trend-Plunge	Reference
1	Talant	47°20'	5°00'	316°-05°	this paper
2	Aillevans	47°35'	6°25'	301°-07°	this paper
3	Seuchey	47°42'	5°31'	301°-05°	this paper
4	Sacquenay	47°35'	5°18'	307°-03°	this paper
5	Clerval	47°23'	6°30'	...	this paper
6	Angirey	47°27'	5°45'	096°-10°	this paper
7	Gy	47°24'	5°50'	301°-08°	this paper
8	Taxenne	47°13'	5°41'	326°-15°	this paper
9	Montagney	47°17'	5°40'	134°-09°	this paper
10	Prauthoy	47°42'	5°18'	131°-01°	this paper
11	St Geosmes	47°49'	5°21'	316°-16°	this paper
12	Chaumont	48°10'	5°10'	312°-12°	this paper
13	Is / Tille	47°32'	5°07'	127°-08°	Bergerat [1987]
14	Gevrey	*	*	270°-04°	Bergerat [1987]
15	Nuits	*	*	092°-13°	Bergerat [1987]
16	...	*	*	091°- *	Bles [1989]
17	...	*	*	096°- *	Bles [1989]
18	Beaune	*	*	139°-10°	Bergerat [1987]
19	Chagny	*	*	099°-24°	Bergerat [1987]
20	...	*	*	115°- *	Coulon [1988]
21	...	*	*	090°- *	Coulon [1988]
22	...	*	*	090°- *	Coulon [1988]
23	...	*	*	098°- *	Coulon [1988]
24	...	*	*	114°- *	Coulon [1988]
25	...	*	*	114°- *	Coulon [1988]
26	Champlitte	47°37'	5°30'	310°-13°	this paper
27	...	*	*	287°-07°	Bergerat [1987]
28	Fouvent	47°38'	5°42'	098°-08°	this paper
29	Brotte	47°36'	5°45'	305°-00°	this paper
30	Vauconcourt	47°39'	5°49'	111°-08°	this paper
31	Scey	47°41'	5°59'	107°-03°	this paper
32	Fretigney	47°29'	5°57'	277°-17°	this paper
33	...	*	*	301°-04°	Bergerat [1987]
34	Courtcuire	47°20'	5°51'	109°-06°	this paper
35	Traitié	47°24'	6°52'	112°-00°	this paper
36	Echenoz	47°33'	6°08'	302°-01°	this paper
37	...	*	*	264°-02°	Bergerat [1987]
38	Mailley	47°33'	6°02'	106°-05°	Bergerat [1987]
39	Saint-Vit	47°11'	5°49'	320°-16°	this paper
40	Seneuil	47°22'	6°32'	105°-03°	this paper
41	Longevelle	47°27'	6°39'	100°-06°	this paper
42	Bussurel	47°32'	6°47'	262°-10°	this paper
43	Dorans	47°35'	6°51'	078°-06°	this paper
44	Denney	47°39'	6°55'	090°-01°	Larroque [1988]
45	...	*	*	094°- *	Larroque [1988]
46	...	*	*	105°- *	Larroque [1988]
47	Altkirch	47°38'	7°13'	269°-09°	this paper
48	Lörrach	47°40'	7°30'	102°-01°	Bergerat [1987]
49	Mulhouse	47°45'	7°23'	090°-00°	Larroque [1988]
50	Freibourg	47°58'	7°40'	285°-01°	Bergerat [1987]
51	Ribeauvillé	48°10'	7°15'	080°-03°	Bergerat [1987]
52	Lahr	48°18'	7°55'	093°-02°	Bergerat [1987]
53	Saverne S	48°31'	7°25'	256°-02°	Bergerat [1987]
54	Saverne N	48°50'	7°35'	091°-01°	Bergerat [1987]
55	Saarburg S	48°43'	7°03'	088°- *	Bergerat [1987]
56	Saarburg N	48°51'	7°05'	090°- *	Bergerat [1987]
57	Ebingen	48°08'	9°10'	101°- *	Bergerat [1987]

Reference papers : Bergerat [1987], Bles et al. [1989], Coulon and Frizon de Lamotte [1988], Lacombe et al. [1990b], Larroque and Laurent [1988]. The "*" indicates the values not given by the authors (σ3 trends and site locations only shown by arrows).

A numerical modeling based on the "distinct element technique" was used to investigate the relationships between the stress perturbations and the Rhine-Saône transform kinematics. This modeling technique is appropriate for studying the behavior of discontinuities in media with uniform or nonuniform rheologies, such as the faulted basement [Dupin, 1990]. The two-dimensional model takes into account the main structural characteristics of the rift-rift transfer: two 20°N trending grabens linked by a 60°N basement fault experiencing discrete slip and acting as a transform. As a consequence of the two-dimensional modeling, the influence of the dip of the basement fault could not be considered, and everything happened as if the fault plane were vertical. However, as horizontal stress perturbations observed in the field worldwide are mainly due to the strike-slip components of fault motion [Ricou, 1978; Rispoli, 1981; Xiaohan, 1983], the results obtained in two-dimensional models in terms of horizontal stress perturbations are still valid. Note that as a consequence of the modeling process, using the distinct element technique (especially the need for maintaining the model cohesion along the basement discontinuity at each time-step), the two-dimensional model does not enable us to check directly our model of oblique opening in the basement.

Numerical characteristics of this modeling and detailed results are discussed in Dupin [1990]. The rheology of the basement was assumed to be elastic, and fault displacements were assumed to follow a Mohr-Coulomb failure criterion. The model was loaded under displacement boundary conditions involving E-W divergence along the east and west sides, whereas the north and south boundaries were submitted to constant confining pressure. Figure 11 displays stress trajectories for this basic model. The modeled direction of extension (minimum horizontal stress axes) is homogeneous in large blocks and near the border faults of the grabens and is consistent with the major E-W extension derived from stress indicators. However, large deviations of σ3 from E-W to NW-SE occur around the transform fault and near the ends of the grabens (Figure 11). This supports the possibility that the Rhine-Saône transform zone, acting during the major crustal extension within the grabens, induced perturbations of the σ3 trajectories very similar to those reconstructed from field data [Dupin, 1990; Dupin and Lacombe, 1991](Figure 5b).

An additional modeling based on the "finite element technique" was performed to extend our understanding of the mechanics of the transform zone and to enhance the interpretation of the paleostress data in the sedimentary cover. This technique assumes that continuous infinitesimal deformation occurs throughout the region, which can include

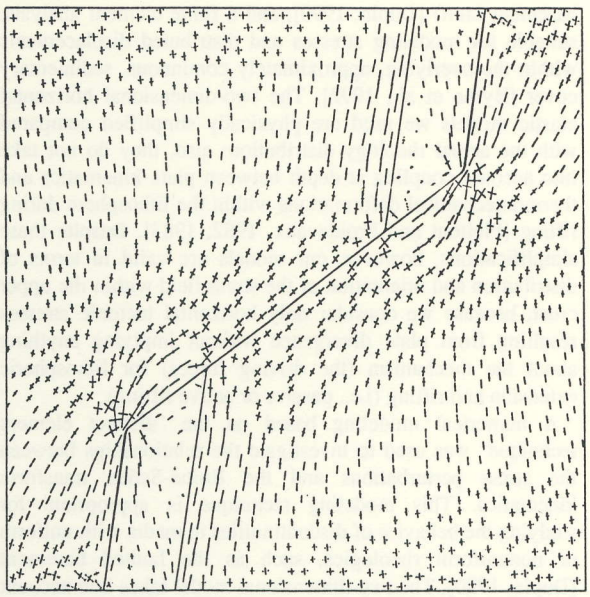

Fig. 11. Distinct element model showing horizontal principal stress axes within the center of the grid. The stress axes do not deviate significantly from the edges of the region shown out to the edge of the grid. For each computed stress tensor, the long and the short axes conventionally represent the maximum and the minimum horizontal stresses, respectively. Note the deviation of extensional stress σ3 from E-W to NW-SE in the western part of the transform. For more details, see text and Dupin [1990].

regions of different rheology or shear strength. The details of this modeling and related experiments are described by Byrne et al. [1992]. An elastic rheology, appropriate as a first approximation for the brittle upper crust, and a simple structural pattern involving two 20°N grabens and a 60°N trending transform zone were considered. It was assumed that the pervasive faulting within the transform zone resulted in increasing weakness relative to the adjacent platform area and that thinning of the crust below the grabens makes them also weaker. The differences in shear strength were approximated by applying different elastic constants for each of these regions (these constants were taken to be consistent with the known amount of crustal stretching within the grabens; in practice, Young's Moduli of 5 GPa within the grabens, 10 to 30 GPa within the transform zone and 50 GPa for the adjacent platform were adopted in calculations). Our models are thus physically simplified, because the strength, as normally understood, refers to the onset of nonelastic behavior and is a different phenomenon from lowered elastic constants. However, the overall conclusions of the modeling will be still valid because a similar (though larger) deformation may be expected with nonelastic rheology (M.H.P. Bott, written communication, 1992).

The finite element model shown in Figure 12 used displacement boundary conditions of E-W extension along the east and west sides and of zero along the north and south boundaries (see Byrne et al, [1992] for details). Remarkably, other models using N-S compression in addition to E-W extension were found to be unable to produce the significant rotation of principal stress axes reconstructed from field data within the transform zone. Figure 12 shows the stress trajectories for the symmetric model. The direction of extension as indicated by the σ3 axes remains nearly E-W across the weaker grabens but experiences significant perturbations around their ends and throughout the transform zone. This simple model shows a general NW-SE directed extension within the transform zone quite similar to the field observations (Figure 5b), and therefore reproduces the general change in stress directions in the vicinity of the transform zone. More elaborate models involving additional details of the transform and graben structure, produce a stress field that fits better the paleostress distribution [Byrne et al., 1992]. We conclude from these finite element models that the stress orientations reconstructed in the Rhine-Saône region may be interpreted in terms of a regional E-W extension with significant perturbations in the transform zone between the two weaker grabens. It is interesting to note that models dominated by N-S compression failed to produce such a perturbed stress field, which confirms our model based on geometrical and structural data (Figure 10b).

Both numerical modelings finally confirm that the observed deviations of σ3 orientations may be simply related to the structure and the kinematics of the Rhine-Saône graben-transform system, involving combined discrete slip in the basement and asymmetric distribution of rheologies in the cover, under a regional stress field dominated by E-W extension.

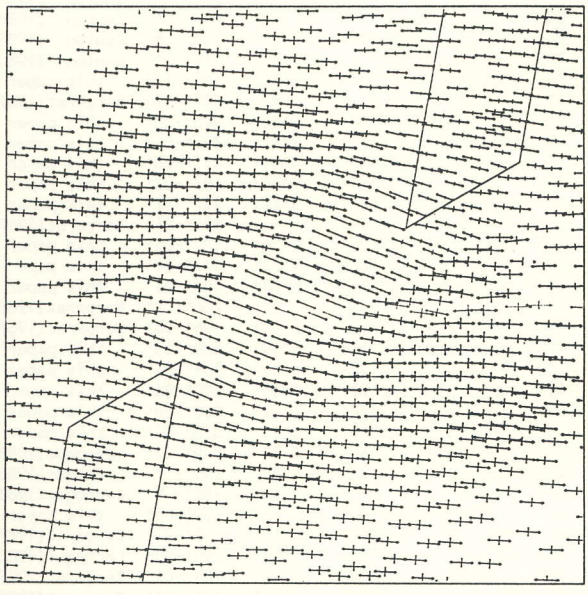

Fig. 12. Finite element model showing horizontal principal stress axes within the center of the grid. The stress axes do not deviate significantly from the edges of the region shown out to the edge of the grid. Arrowheads differentiate compressive and extensive stress axes. Lengths of axes are proportional to stress magnitudes. This simple model reproduces the essential features observed in the paleostress data, most notably the rotation of the minimum horizontal stress axes from E-W trends outside the transform zone to NW-SE within it. For more details, see text and Byrne et al. [1992].

DISCUSSION AND CONCLUSIONS

During the main Cenozoic subsidence of the continental Rhine and Saône grabens, in response to E-W lithospheric extension, a major Permo-Carboniferous basement fault system, trending 60°N, was reactivated as a left-lateral/extensional transform zone connecting the two grabens. This oblique reactivation induced transtensive distributed deformation in the overlying sedimentary cover along numerous oblique-slip en échelon faults. Following previous works, which already emphasized the influence of ancient structures on rifting [e.g., Illies, 1981; Daly et al., 1989], this provides further evidence that preexisting fractures and zones of weakness in the continental crust can be reactivated during rifting and control localization of continental rift-transform systems. The dependence of continental transform zones on inherited structures explains why they tend to form larger and more complex shear zones than oceanic transform faults and may not be perpendicular to the rift segments and parallel to the direction of major extension.

The trend of $\sigma 1$ orientations related to the initial Paleocene-Eocene Pyrenean-Alpine compressional phase is very homogeneous in the area investigated, and no significant large-scale perturbations could be detected (Figure 2). On the other hand, the Rhine-Saône transform kinematics was associated with regional-scale perturbations of extensional stress trajectories (Figures 3 and 5b). Numerical modeling indicates that boundary conditions of actual E-W extension are required to account for these perturbations. This leads to the conclusion that no significant transform motion occurred during the preextensional N-S Eocene compression. It also suggests that the stress regime prevailing during the whole of the development of the Rhine-Saône rift-transform system was predominantly extensional rather than compressional. This portion of the west European Rift consequently did not entirely originate in response to N-S compression due to convergence between Africa and Eurasia (Alpine/Pyrenean compression). Although this convergence may have played an indirect role [Sengör, 1976; Tapponnier, 1977; Illies and Greiner, 1978], the Rhine-Saône rift system rather resulted from regional tensional stresses and coeval E-W extension along preexisting zones of crustal weakness. This conclusion is in agreement with the recent plate kinematics reconstructions of Europe implying that the entire west European Rift developed under pure extension due to E-W divergent motion between westernmost Europe and the rest of Eurasia during the Oligocene [Le Pichon et al., 1988]. This dominant E-W extension also accounts for the abundance of extensional features of Oligocene age that can be found within and away from the west European Rift system [e.g., Coulon and Frizon de Lamotte, 1988].

The model we finally propose for the Oligocene tectonics and kinematics of the Rhine-Saône transform zone takes into account most of the geometric constraints raised from structural and paleostress analyses. It accounts for the nearly synchronous opening of the Saône and Rhine continental rifts, the large-scale perturbations of extensional stress trajectories, and the development of a typical en échelon wrench /extensional fault pattern in the sedimentary cover of the Rhine-Saône transform zone, and takes into account the influence by structural heterogeneities in the brittle continental crust. The Rhine-Saône transform zone thus appears to be a major, Hercynian-inherited, zone of crustal weakness that localized deformation and reoriented tectonic stress during Oligocene extension.

APPENDIX

A simple geometrical model of stress-slip relationships for a preexisting fault plane can be used in order to determine the slip vector, following the assumption of Wallace [1951] and Bott [1959] that slickenlines on a fault plane are parallel to the maximum shear stress. Let us consider a single fault plane of given orientation submitted to homogeneous stress. In our case, the minimum stress $\sigma 3$ is horizontal and trends E-W. Considering the Oligocene tectonism (see text), the maximum compressional stress $\sigma 1$ is generally vertical (normal faulting regime). The orientation of shear (and slip) on preexisting faults not only depends on the fault orientation with respect to the new stress field but is also a function of the ratio $\Phi = (\sigma 2 - \sigma 3)/(\sigma 1 - \sigma 3)$ between principal stresses. As pointed out by Angelier [1984], substituting values of 1, Φ, and 0 for principal stress magnitudes $\sigma 1$, $\sigma 2$, and $\sigma 3$, respectively, does not affect the orientation and sense of shear on any plane. In the case considered herein, $\Phi = 0$ corresponds to multidirectional extension ($\sigma 1$ vertical, with $\sigma 2 = \sigma 3$), whereas $\Phi = 1$ corresponds to uniaxial extension ($\sigma 3$ horizontal trending E-W, with $\sigma 1 = \sigma 2$). Values between 0 and 1 correspond to normal fault regime ($\sigma 1$ vertical, $\sigma 3$ horizontal trending E-W).

The stress tensor T being thus defined, with principal values 1 (vertical stress), Φ (N-S horizontal axis) and 0 (E-W horizontal axis), one may easily compute the stress $\vec{\sigma}$ exerted on any fault plane whose unit normal vector is $\vec{n}$ ($\vec{\sigma} = T\,\vec{n}$). Then the normal stress, $\vec{\nu}$, is given by $\vec{\nu} = \vec{n}\,(\vec{\sigma}.\vec{n})$, and finally the shear stress, $\vec{\tau}$, is given by $\vec{\sigma} = \vec{\nu} + \vec{\tau}$. Components of $\vec{\sigma}$ along reference axes (E-W, N-S and vertical) are thus obtained as a simple linear functions of Φ (Figure A1).

1. For a fault plane which strikes 30°N and dips 80° to the S-SE (upper row of Figure A1), the expected slip varies from dip-slip (for $\Phi = 0$) to oblique-slip (normal left-lateral) with a decreasing pitch of 35°N for $\Phi = 0.5$ and of 17°N for $\Phi = 1$. This situation is typical for steeply dipping faults inherited from the Eocene compressional event (former left-lateral strike-slip faults). Our calculation suggests that such faults are reactivated as oblique-slip faults (normal sinistral) with pitches of slickenside lineations ranging from 90° to 35° to the north as $\sigma 2$ varies from $\sigma 3$ ($\Phi = 0$) to $0.5(\sigma 1 + \sigma 3)$ ($\Phi = 0.5$). Values of Φ ranging from 0 to 0.5 are common in the Rhine-Saône transform zone, as stress tensor determinations indicate (see Table 1).

2. For a fault plane which strikes 60°N and dips 30° to the S-SE (second row of Figure A1), similar results are obtained in terms of sense of motion, but critical pitch values differ. For a Φ ratio varying from 0 to 0.5 as before, the pitch of the expected slip vector remains very large (90° to 78°N), indicating that the left-lateral component of motion on such faults should be expected to be very small. For values of Φ ranging from 0.5 to 1, the pitch decreases rapidly, from 78° to 27°N (Figure A1).

3. For a fault plane that also strikes 60°N but dips steeper, 60° to the S-SE (lower row of Figure A1), similar results are

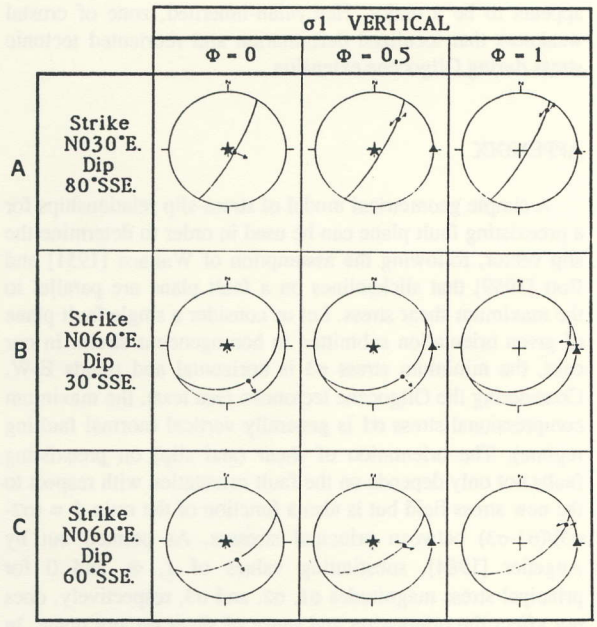

Fig. A1. Direction and sense of theoretical slip motion along fault planes with various strikes and dips as functions of the Φ ratio.

obtained: the pitch of normal-sinistral motion varies from 90° to 55°N and 16°N as Φ varies from 0 to 0.5 and to 1 (Figure A1).

The last two determinations suggest that for faults that trend 60°N, variations in dip within the approximate range 30°-60° have little effect on fault slip direction (however, dip variation may strongly influence friction). For reasonable values of Φ (between 0 and 0.5, as indicated by stress determinations), fault motion is predominantly normal, with a minor but significant left-lateral component. This result is crucial, because the real nature of inherited basement faults, hence their dip, remains unknown. The 30° dips are common for reverse faults, whereas the 60° dips are common for normal faults. The present knowledge of the Hercynian structure shows that both types may exist along common E-NE-W-SW trends.

Acknowledgments. Field work and data analysis were supported by the Institut Français du Pétrole. The authors thank Lee Jian-Cheng, who kindly provided the spatial averaging program used in Figure 5b. G. Eisbacher, P.A. Ziegler, and C. Ebinger are also thanked for their thorough reviews and their constructive comments which allowed improvement of the manuscript.

REFERENCES

Angelier, J., Tectonic analysis of fault slip data sets, *J. Geophys. Res., 89*, (B7), 5835-5848, 1984.

Angelier, J., From orientation to magnitudes in paleostress determinations using fault slip data, *J. Struct. Geol., 11*, 37-50, 1989.

Angelier, J., Inversion of field data in fault tectonics to obtain the regional stress. III: A new rapid direct inversion method by analytical means, *Geophys. J. Int., 103*, 363-376, 1990.

Arthaud, F., and P. Matte, Les décrochements tardi-hercyniens du Sud-Ouest de l' Europe. Géométrie et essai de reconstitution des conditions de la déformation, *Tectonophysics, 25*, 139-171, 1975.

Arthaud, F., and P. Matte, Late Paleozoic strike-slip faulting in southern Europe and northern Africa : Result of a right-lateral shear zone between the Appalachians and the Urals, *Geol. Soc. Am. Bull., 88*, 1305-1320, 1977.

Arthaud F. and M. Seguret, Les structures pyrénéennes du Languedoc et du Golfe du Lion (Sud de la France), *Bull. Soc. Géol. Fr., 7*, (23,1), 51-63, 1981.

Bergerat, F., La fracturation de l'avant-pays jurassien entre les fossés de la Saône et du Rhin. Analyse et essai d'interprétation dynamique, *Revue Géog. Phys. Géol. Dynam.*, Paris, (2), XIX, *4*, 325-338, 1977.

Bergerat, F., Stress fields in the European platform at the time of Africa-Eurasia collision, *Tectonics, 6*, 99-132, 1987.

Bergerat, F., and J. Chorowicz, Etude des images Landsat de la zone transformante Rhin-Saône (France), *Geol. Rundsch., 70*, (1), 354-367, 1981.

Bergerat, F., J.L. Mugnier, S. Guellec, C. Truffert , M. Cazes, M. Damotte and F. Roure, Extensional tectonics and subsidence of the Bresse basin : A view from ECORS data, In "*Deep structures of the Alps*", *Mém. Soc. Géol. France*, edited by F. Roure, P. Heitzmann and R. Polino, *156*; (1), 145-156, 1990.

Bles, J.L., D. Bonijoly, C. Castaing and Y. Gros, Successive post-Variscan stress fields in the French Massif Central and its borders (western European plate): Comparison with geodynamic data, *Tectonophysics, 169*, 79-111, 1989.

Bott, M.H.P., The mechanism of oblique slip faulting, *Geol. Mag., 96*, (2), 109-117, 1959.

Byrne, D., J. Angelier, O. Lacombe and J.M. Dupin, Finite element model of the mechanics of the Rhine-Saône transform zone, *Int. rep. Inst. Franç. Pétr.* n° 39824 *Mécanique des milieux discontinus et reconstitution des contraintes*, p. 77, 1992.

Caire, A., Caractères et conditions du recouvrement tectonique pontien dans la partie occidentale du faisceau salinois (Jura). Les décrochements jurassiens dans le cadre alpin, *Actes du 99e Congr. Soc. Sav.*, Besançon, *1*, 73-84, 1974.

Carey, E., and B. Brunier, Analyse théorique et numérique d'un modèle mécanique élémentaire appliqué à l'étude d'une population de failles, *C. R. Acad. Sci.*, Paris, (D), *279*, 891-894, 1974.

Celerier, B., How much does slip on a reactivated fault plane constrain the stress tensor ?, *Tectonics, 7*, 6, 1257-1278, 1988.

Chauve, P., J. Martin, E. Petitjean and F. Sequeiro, Le chevauchement du Jura sur la Bresse. Données nouvelles et réinterprétation des sondages, *Bull. Soc. Géol. Fr.* (8), IV, *5*, 861-870, 1988.

Chorowicz, J., Transfer and transform fault zones in continental rifts : examples in the Afro-arabian rift system. Implication on crust breaking, *J. Afric. Earth Sci., 8*, 2-4, 203-214, 1989.

Contini, D., and N. Theobald, Relations entre le fossé rhénan et le fossé de la Saône. Tectonique des régions sous-vosgiennes et préjurassiennes, In *Approaches to Taphrogenesis, Sci. Rep. 8*, edited by J.H. Illies and K. Fuchs, 309-321, Stuttgart, 1974.

Coulon, M., and D. Frizon de Lamotte, Les extensions cénozoiques dans l'Est du bassin de Paris: Mise en évidence et interprétation, *C. R. Acad. Sci.*, Paris, *307*, II, 1113-1119, 1988.

Daly, M.C., J. Chorowicz and J.D. Fairhead, Rift basin evolution in Africa: the influence of the reactivated steep basement shear zones, In "*Inversion tectonics*", *Geol. Soc. Spec. Publ. London*, edited by M.A. Cooper and G.D. Williams, *44*, 309-334, 1989.

De Charpal, O., P. Tremolieres, F. Jean and P. Masse, Un exemple de tectonique de plate-forme: les Causses majeures (Sud du Massif Central, France), *Revue Inst. Franç. Pétr.*, Paris, *29*, (5), 641-659, 1974.

Dewey, J.F., and B.F. Windley, Paleocene-Oligocene tectonics of NW Europe, In "*Early Tertiary Volcanism and the opening of the NE Atlantic*", *Geol. Soc. Spec. Publ. London,* edited by *A.C.* Morton and L.M. Parson, *39*, 25-31, 1988.

Dupin, J.M., Modélisation numérique de la déformation discontinue: application de la méthode des éléments distincts aux jeux de failles (3D) et à la distribution des contraintes autour d'une zone transformante intracontinentale (2D), D.E.A, Univ. Pierre et Marie Curie, Paris, 88 pp, 1990.

Dupin, J.M., and O. Lacombe, Paleostress evolution and kinematics of the Rhine-Saône continental "transform zone" : II. Numerical modelling., *Terra Nova,* E.U.G VI, Abstract Volume, Strasbourg, p. 371, 1991.

Ebinger, C.J., Geometric and kinematic development of border faults and accommodation zones, Kivu-Rusizi, Africa, *Tectonics, 8,* 117-133, 1989.

Edel, J.B., and P. Fluck, The upper Rhenish Shield basement (Vosges, upper Rhinegraben and Schwarzwald): main structural features deduced from magnetic, gravimetric and geological data, *Tectonophysics, 169*, 303-316, 1989.

Edel, J.B., K. Fuchs, C. Gelbke and C. Prodehl, Deep structure of the southern. Rhinegraben area from seismic-refraction investigations, *J. Geophys., 41*, 333-356, 1975.

Eisbacher, G.H., E. Lüschen and F. Wickert, Crustal-scale thrusting and extension in the Hercynian Schwarzwald and Vosges, Central Europe, *Tectonics, 8*, 1-21, 1989.

Elmohandes, S.E., The Central European Graben system: Rifting imitated by clay modeling, *Tectonophysics, 73*, 69-78, 1981.

Etchecopar, A., Etude des états de contraintes en tectonique cassante et simulation de déformations plastiques (approche mathématique), Thèse de Doctorat d'état-ès-Sciences, Univ. Sciences et Techniques du Languedoc, Montpellier, 270 pp, 1984.

Etchecopar, A., and M. Mattauer, Méthodes dynamiques d'analyse des populations de failles, *Bull. Soc. Géol. Fr., 8*, 289-302, 1988.

Etchecopar, A., G. Vasseur and M. Daignieres, An inverse problem in microtectonics for the determination of stress tensor from fault striation analysis, *J. Struct. Geol., 3*, 51-65, 1981.

Fleitout, L., and C. Froidevaux, Tectonics and topography for a lithosphere containing density heterogeneities, *Tectonics, 1*, 21-56, 1982.

Fleitout, L., and C. Froidevaux, Tectonic stresses in the lithosphere, *Tectonics, 2*, 315-324, 1983.

Freund, R., Kinematics of transform and transcurrent faults, *Tectonophysics, 21*, 93-134, 1974.

Garfunkel, Z., Internal structure of the Dead Sea leaky transform (rift) in relation to plate kinematics, *Tectonophysics, 80*, 81-108, 1981.

Gelard, J.P., Coulissements horizontaux dans les calcaires jurassiques de Talant (près de Dijon) et preuves microtectoniques du caractère polyphasé de la fracturation en Bourgogne, *Bull. Soc. Géol. Bourgogne, 32*, (2), 59-69, 1979.

Guellec, S., D. Lajat, A. Mascle, F. Roure and M.Tardy, Deep seismic profiling and petroleum potential in the western Alps : constraints with ECORS data, balanced cross sections and hydrocarbon modeling, In "*The Potential of Deep Seismic Profiling for Hydrocarbon Exploration*", edited by B. Pinet and C. Bois, Technip, 425-437, 1990.

Illies, J.H., The Rhinegraben rift system-plate tectonics and transform faulting, *Geophys. Surv., 1*, 27-60, 1972.

Illies, J.H., Taphrogenesis and plate tectonics, In "*Approaches to Taphrogenesis*", edited by J.H. Illies and K. Fuchs, Sci. Rep. 8, Verlag, Stuttgart, 433-460, 1974.

Illies, J.H., Mechanism of graben formation, *Tectonophysics, 73*, 249-266, 1981.

Illies, J.H. and G. Greiner, Rhinegraben and the Alpine system, *Geol. Soc. Am. Bull., 89*, 770-782, 1978.

Kazmin, V., Transform faults in the African Rift System, In "*Geodynamic Evolution of the Afro-Arabic rift system*", Roma, *Atti. Accad. Naz. Lincei Mem., 9*, 65-73, 1980.

Lacombe, O., Maclage, fracturation et paléocontraintes intraplaques: Application à la plate-forme carbonatée ouest-européenne, Thèse de Doctorat-ès-Sciences, Mém. Sci. Terre de l'Université Pierre et Marie Curie, 316 pp, 1992.

Lacombe, O., and J.M. Dupin, Paleostress evolution and kinematics of the Rhine-Saône continental "transform zone": I. Field data, *Terra Nova,* E.U.G VI, Abstract Volume, Strasbourg, p. 370, 1991.

Lacombe, O., J. Angelier, F. Bergerat and P. Laurent, Tectoniques superposées et perturbations de contrainte dans la zone transformante Rhin-Saône: Apport de l'analyse des failles et des macles de la calcite, *Bull. Soc. Géol. Fr.,* VI, *5*, 853-863, 1990a.

Lacombe, O., J. Angelier and P. Laurent, Determining paleostress orientations from faults and calcite twins: A case study near the Sainte-Victoire Range (southern France), *Tectonophysics, 201*, 141-156, 1992.

Lacombe, O., J. Angelier, P. Laurent, F. Bergerat and C. Tourneret, Joint analyses of calcite twins and fault slips as a key for deciphering polyphase tectonics: Burgundy as a case study, *Tectonophysics, 182*, 279-300, 1990b.

Larroque, J.M., and M. Ansart, Les déformations liées à la tectonique distensive oligocène du bassin potassique de Mulhouse: cas du secteur minier, *Bull. Soc. géol. Fr.*, I, *6*, 837-847, 1985.

Larroque, J.M., and P. Laurent, Evolution of the stress field pattern in the south of the Rhine graben from the Eocene to the present, *Tectonophysics, 148*, 41-58, 1988.

Laubscher, H.P., Grundsätzliches zur Tektonik des Rhein Graben. In "*Graben Problems*", Int. Upper Mantle Project, edited by J.H. Illies and S. Müller, Sci. Rep. 27, Schweizerbart, Stuttgart, 79-87, 1970.

Le Pichon, X., F. Bergerat and M.J. Roulet, Plate kinematics and tectonics leading to Alpine belt formation: A new analysis, In "*Processes in Continental Lithospheric Deformation*", *Geol. Soc. Am. Spec. Pap., 218*, 111-131, 1988.

Letouzey, J., Cenozoic paleo-stress pattern in the Alpine foreland and structural interpretation in a platform basin, *Tectonophysics, 132*, 215-231, 1986.

Letouzey, J., and P. Tremolieres, Paleo-stress fields around the Mediterranean since the Mesozoic derived from microtectonics: comparisons with plate tectonic data, In "*Géologie des chaînes alpines issues de la Téthys*", *Mém. Bur. Rech. Géol. Min.*, 115, 261-273, 1980.

Mattauer, M., and J.L. Mercier, Microtectonique et grande tectonique, *Mém. Hors Sér. Soc. Géol. Fr., 10*, 141-161, 1980.

Matte, P., La chaîne varisque parmi les chaînes paléozoiques péri-atlantiques: modèle d'évolution et position des grands blocs continentaux au Permo-Carbonifère, *Bull. Soc. Géol. Fr.*, II, *1*, 9-24, 1986a.

Matte, P., Tectonics and plate tectonics model for the Variscan Belts of Europe, *Tectonophysics, 126*, 329-374, 1986b.

Müller, W.H., M. Huber, A. Isler and P. Kleboth, Erläuterung zur "Geologischen Karte der zentralen Nordschweiz 1/100 000e", *NAGRA Tech. Ref. (NAGRA)*, 84-25, 234 pp, 1984.

Rat, P., Le système Bourgogne-Morvan-Bresse (articulation entre le bassin parisien et le domaine péri-alpin). In "*Géologie de la France*", edited by J. Debelmas, Vol.II, Doin, Paris, 480-500, 1974.

Rat, P., Structures et phases de structuration dans les plateaux bourguignons et le Nord-Ouest du fossé bressan (France), *Geol. Rundsch., 65*, Stuttgart, 101-126, 1976.

Rat, P., Les phases tectoniques au Tertiaire dans le Nord du fossé bressan et ses marges bourguignonnes en regard des systèmes d'érosion et sédimentation, *C. R. Somm. Soc. Géol. Fr., 5*, 231-234, 1978.

Ricou, L.E., Accidents régulateurs de contrainte et réorientation de contrainte, *C. R. Acad. Sci., 286*, 1657-1660, 1978.

Rispoli, R., Stress fields about strike-slip faults inferred from stylolites and tension gashes, *Tectonophysics, 75*, 29-36, 1981.

Ron, H., and Y. Eyal, Intraplate deformation by block rotation and mesostructures along the Dead Sea transform, northern Israel, *Tectonics, 4*, 85-105, 1985.

Segall, P., and D.D. Pollard, Mechanics of discontinuous faults, *J. Geophys. Res., 85*, 4337-4387, 1980.

Sengör, A.M.C., Collision of irregular continental margins: Implications for foreland deformation of Alpine-type orogens, *Geology, 4*, 779-782, 1976.

Tapponnier, P., Evolution tectonique du système alpin en Méditerranée: Poinçonnement et écrasement rigide-plastique, *Bull. Soc. Géol. Fr.*, XIX, 437-460, 1977.

Tapponnier, P., and J. Varet, La zone de Mak'arrasou en Afar: un équivalent émergé

des failles transformantes océaniques, *C. R. Acad. Sci.*, 278, (D), 209-214, 1974.

Tourneret, C., and P. Laurent, Paleostress orientations from calcite twins in the north pyrenean foreland, determined by the Etchecopar inverse method, *Tectonophysics, 180*, 287-302, 1990.

Tron, V., and J.P. Brun, Experiments on oblique rifting in brittle-ductile systems, *Tectonophysics, 188*, 71-84, 1991.

Villemin, T., Tectoniques en extension, subsidence et fracturation: Le fossé rhénan et le bassin sarro-lorrain, Thèse de Doctorat-ès-Sciences, Mém. Sci. Terre Univ. Pierre et Marie Curie, 270 pp, 1986.

Villemin, T., and F. Bergerat, L'évolution structurale du fossé rhénan au cours du Cénozoique: Un bilan de la déformation et des effets thermiques de l'extension, *Bull. Soc. Géol. Fr.*, III, *2*, 245-255, 1987.

Wallace, R.E., Geometry of shearing stress and relation to faulting, *J. Geol., 59*, 118-130, 1951.

Wickert, F., and G.M. Eisbacher, Two-sided Variscan thrust tectonics in the Vosges Mountains, northeastern France, *Geodyn. Acta, 2*, 101-120, 1988.

Xiaohan, L., (I) Perturbations de contraintes liées aux structures cassantes dans les calcaires fins du Languedoc, Observations et simulations mathématiques, (II) Mesure de la déformation finie à l'aide de la méthode Fry, Application aux gneiss des Bormes (massif des Maures), Thèse de Doctorat-ès-Sciences, Univ. Sciences et Techniques du Languedoc, Montpellier, 152 pp, 1983.

Ziegler, P.A., Northwestern Europe: Subsidence patterns of post-variscan basins, In "*Geology of Europe from Precambrian to the post-Hercynian sedimentary basins*", edited by Bur. Rech. Géol. Min. and Soc. Géol. Nord, 249-280, 1980.

Ziegler, P.A., Geodynamic model for the Paleozoic crustal consolidation of western and central Europe, *Tectonophysics, 126*, 303-328, 1986.

Ziegler, P.A., Evolution of the Arctic-North Atlantic and the western Tethys, *Mem. Am. Assoc. Petrol. Geol., 43*, 198 pp, 1988.

Ziegler, P.A., Geological Atlas of Western and Central Europe, 2nd ed., edited by Shell International Petroleum , the Hague, 239 pp, 1990.

Ziegler, P.A., European Cenozoic rift system, In "*Geodynamics of Rifting, Vol I. Case History Studies on Rifts : Europe and Asia*", edited by P.A. Ziegler, *Tectonophysics, 208*, 91-111, 1992.

J. Angelier, D. Byrne, J.-M. Dupin, and O. Lacombe, Tectonique Quantitative, Université Pierre et Marie Curie, Tour 26-25 E1, Boîte 129, 4, place Jussieu, 75252 Paris Cedex 05, France.

(Received December 9, 1991; revised November 19, 1992; accepted January 5, 1993.)